Journal of Applied Electrochemistry **31**: 629–639, 2001.

Reduction of metal ions in dilute solutions using a GBC-reactor Part II: Theoretical model for the hydrogen oxidation in a gas diffusion electrode at relatively low current densities

I. PORTEGIES ZWART[1,2], J.K.M. JANSEN[3] and L.J.J. JANSSEN[1]
[1]*Eindhoven University of Technology, Department of Chemical Engineering, Laboratory of Process Development, STO 3.48, 5600 MB Eindhoven, The Netherlands*
[2]*Present address: CORUS RD&T, PO Box 10000, 1970 CA IJmuiden, The Netherlands*
[3]*Department of Mathematics, Scientific Computing Group, PO Box 513, 5600 MB Eindhoven, The Netherlands*

Received 24 November 1998; accepted in revised form 9 January 2001

Key words: gas diffusion electrode, GBC-reactor, hydrogen oxidation, Volmer–Tafel mechanism

Abstract

The GBC-reactor is based on the combination of a gas diffusion anode and a porous cathode. A theoretical model for gas diffusion electrode, valid at relatively low current densities, is derived. This is based on the pseudohomogeneous film model including an approximation of the Volmer–Tafel mechanism for the hydrogen oxidation kinetics. Results show a severe mass transfer limitation of the hydrogen oxidation reaction inside the active layer of the gas diffusion electrode, even at low current densities. Empirical formulae are given to estimate whether leakage of dissolved hydrogen gas into the bulk electrolyte occurs at specific process conditions. A simplified version of the model, the reactive plane approximation, is presented.

List of symbols

a_e	specific surface area ($m^2\ m^{-3}$)
Bi_m	Biot mass number (–): $k_{d,H_2} L/D_{H_2,eff}$
c	concentration (mol m^{-3})
D	diffusion coefficient ($m^2\ s^{-1}$)
E	electrode potential (V)
F	faradaic constant (96 487 C mol^{-1})
i	reaction current density (A m^{-2})
i_0	exchange current density (A m^{-2})
j	current density based on geometric surface area (A m^{-2})
j_0	exchange current density based on geometric surface area (A m^{-2})
$K1$, $K2$	dimensionless parameters as defined by Equation 28
k_d	external solution phase mass transfer coefficient (m s^{-1})
k_{Td}	reaction rate constant dissociation Tafel step (m s^{-1})
k_{Tr}	reaction rate constant recombination Tafel step (mol $m^{-2}\ s^{-1}$)
$k^a_{V,0}$	equilibrium reaction rate constant anodic Volmer step (mol $m^{-2}\ s^{-1}$)
$k^c_{V,0}$	equilibrium reaction rate constant cathodic Volmer step (m s^{-1})
L	thickness of gas diffusion electrode active layer (m)
R	gas constant (8.314 J $mol^{-1}\ K^{-1}$)
T	temperature (K)

Greek symbols

Φ	electric potential (V)
Γ	fractional conversion
α	anodic transfer coefficient
ε	porosity
γ, γ^*	concentration order
η	electrode overpotential (V)
κ	solution conductivity ($\Omega^{-1}\ m^{-1}$)
λ	dimensionless penetration depth
θ	fractional surface coverage of adsorbed hydrogen atoms
ξ	dimensionless distance

Sub- and superscript

*	dimensionless parameter
□	standard state
0	equilibrium state
app	apparent
m	matrix/solid phase
macro	macroscopic quantity
ref	reference condition corresponding with equilibrium state
s	solution phase
T	Tafel reaction
V	Volmer reaction

1. Introduction

For the reduction of metal ions in dilute solutions a new type of electrochemical reactor called the 'gas diffusion electrode packed bed electrode cell' (GBC-reactor), was proposed by Janssen [1, 2]. The reactor consists of a gas diffusion anode coupled, via direct or indirect contact, with a porous cathode (e.g., a packed bed electrode [1–5]). Different reactor configurations and their applications have been discussed by Portegies Zwart and Janssen [3]. The working principle of the reactor is based upon two main reactions: the catalytic oxidation of hydrogen gas in the gas diffusion anode (Equation 1) and the simultaneous reduction of metal ions in the porous cathode (Equation 2): That is,

$$H_2 \leftrightarrow 2H^+ + 2e^- \quad (1)$$

$$M^{m^+} + ne^- \leftrightarrow M^{(m-n)+} \quad (2)$$

When the Gibbs free energy change of these combined reactions is negative then the oxidative and reduction processes occur spontaneously, without the need for an external power supply.

A detailed GBC-reactor model must consider the behaviour of the gas diffusion electrode. In this work a theoretical model for the gas diffusion electrode is described, which is based on a pseudohomogeneous film model including an approximation of the Volmer–Tafel mechanism for the hydrogen oxidation reaction. Results show a severe mass transfer limitation of the hydrogen oxidation reaction inside the active layer of the gas diffusion anode even at low current densities. Empirical formulae were formulated which indicate whether leakage of dissolved hydrogen gas into the bulk solution will occur at specific process conditions. An adapted, simplified version of the model is also presented, indicated as the reactive plane approximation.

2. Theory

2.1. General considerations and major assumptions

The gas diffusion electrodes used in the GBC-process are fuel cell grade electrodes [1–6] commonly applied in phosphoric acid fuel cells (PAFCs). These electrodes consist of a hydrophobic porous backing for gas transport and a hydrophilic porous active layer in which dissolved hydrogen reacts on catalytic sites distributed over the solid phase.

The fact that in the GBC-process the gas diffusion electrode is fed with pure hydrogen gas combined with the expectation that the hydrogen oxidation current densities will be relatively low during reactor operation, leads to the conclusion that mass transfer of hydrogen gas in the porous backing will not be important [3]. Thus, only the behaviour of the active layer needs to be described. Generally, for the active layer a choice is made between a version of the so-called agglomerate model (e.g., [7, 8]) or the pseudohomogeneous film model (e.g., [9–11]). The agglomerate model uses many adjustable parameters, which are difficult to determine. Therefore, the pseudohomogeneous film model is used, incorporating appropriate hydrogen oxidation kinetics.

The formulated model is presented schematically in Figure 1. On the liquid side of the gas diffusion electrode an external mass transfer resistance is considered. At the gas–liquid interface equilibrium is maintained, due to the fast mass transfer in the gas phase, and gas and liquid phase concentrations are linked by the Henry coefficient. The gas diffusion electrode is operated in a strongly acidic environment, thus a constant proton concentration is assumed in all circumstances. Further important assumptions/conditions are: (i) that the electrode operates in a steady state under isothermal conditions at 298 K; (ii) that the porosity and specific surface area of the electrode are uniform; (iii) that the conductivity of the solid phase is very good, so it is equipotential; (iv) that the gas feed exists of pure hydrogen gas at atmospheric pressure; (v) that a high concentration of acidic electrolyte is used, 1 kmol m^{-3} of H_2SO_4, so ionic migration can be neglected; and finally (vi) that only lateral gradients exist, so an one-dimensional model suffices.

2.2. Hydrogen oxidation kinetics

The mechanism of hydrogen oxidation on the platinum catalysed gas diffusion electrode is described according to the Volmer–Tafel mechanism [12–14].

$$H_2 \underset{k_{Tr}}{\overset{k_{Td}}{\rightleftharpoons}} 2\,H_{ad} \quad \text{Tafel reaction} \quad (3)$$

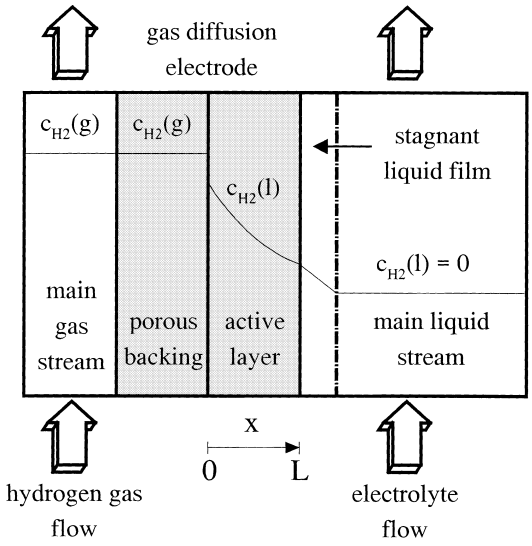

Fig. 1. Schematic presentation of the pseudohomogeneous film model for the active layer of the gas diffusion electrode, showing the course of the concentration profile of molecular hydrogen in the gas and liquid phase.

$$H_{ad} \underset{k_V^c}{\overset{k_V^a}{\rightleftharpoons}} H^+ + e^- \quad \text{Volmer reaction} \tag{4}$$

Vermeijlen et al. [13] showed that the rate determining step in this mechanism depends on the reactivity of the gas diffusion anode. The Volmer reaction is rate controlling in case of high reactivity, the Tafel reaction in case of low reactivity.

Intermediate reactive anodes will be affected by both mechanisms. The Tafel and Volmer reaction current densities are expressed, respectively, as [13, 14]:

$$i_T = i_{0,T}\left(\left(\frac{1-\theta}{1-\theta_0}\right)^2 - \left(\frac{\theta}{\theta_0}\right)^2\right) \tag{5}$$

$$i_V = i_{0,V}\left(\left(\frac{\theta}{\theta_0}\right)\exp\left[\alpha_V \frac{F}{RT}\eta\right] - \left(\frac{1-\theta}{1-\theta_0}\right)\exp\left[-(1-\alpha_V)\frac{F}{RT}\eta\right]\right) \tag{6}$$

The Tafel and Volmer exchange current density are given by Equations 7 and 8. The observed reaction current density is given by Equation 9.

$$i_{0,T} = 2Fk_{Td}(1-\theta_0)^2 c_{H_2}^{ref} = 2Fk_{Tr}{\theta_0}^2 \tag{7}$$

$$i_{0,V} = Fk_{V,0}^a \exp\left[\alpha_V \frac{F}{RT}E_0\right]\theta_0 = Fk_{V,0}^c \exp\left[-(1-\alpha_V)\frac{F}{RT}E_0\right](1-\theta_0)c_{H^+}^{ref} \tag{8}$$

$$i = i_T = i_V \tag{9}$$

Using Equations 5–9, extended with certain limiting situations (i.e., Tafel limiting current density, diffusion limiting current density), it is possible to calculate the reaction current density as a function of electrode potential [13]. In this case a modified model, based on limiting conditions, is used to express the relation between the reaction current density and the electrode potential for the Tafel–Volmer mechanism. This means that either the Tafel or Volmer reaction is the rate determining step, combined with either a very high or low fractional surface coverage of adsorbed hydrogen atoms ($\theta \to 1$ or $\theta \to 0$).

2.2.1. *Tafel reaction rate determining step*

The Volmer reaction is considered to be in quasi-equilibrium, so from Equation 6 we can derive Equation 10. This expression can be substituted into Equation 5 to give, after some rearrangement, Equation 11 which can be linearized for small values of the overpotential to give Equation 12.

$$\frac{\theta}{\theta_0} = \frac{1-\theta}{1-\theta_0}\exp\left[-\frac{F}{RT}\eta\right] \tag{10}$$

$$i = i_{0,T}\left(\frac{1-\theta}{1-\theta_0}\right)^2\left(1-\exp\left[-\frac{2F}{RT}\eta\right]\right) \tag{11}$$

$$i = 2i_{0,T}\left(\frac{1-\theta}{1-\theta_0}\right)^2\frac{F}{RT}\eta \tag{12}$$

Consideration of Equations 12 and 7 reveals that in the case of a very low fractional surface coverage the current density will be directly proportional to the dissolved hydrogen concentration. Otherwise, if the fractional surface coverage becomes very high then the current density will become almost independent on the dissolved hydrogen concentration.

2.2.2. *Volmer reaction rate-determining step*

In this case the Tafel reaction is considered to be in quasi-equilibrium, so from Equation 5 we can derive Equation 13. Using the latter, Equation 6 can be transformed to Equation 14, which can be linearized for small η (Equation 15). So,

$$\frac{\theta}{\theta_0} = \frac{1-\theta}{1-\theta_0} \tag{13}$$

$$i = i_{0,V}\left(\frac{\theta}{\theta_0}\right)\left(\exp\left[\alpha_V\frac{F}{RT}\eta\right] - \exp\left[-(1-\alpha_V)\frac{F}{RT}\eta\right]\right) \tag{14}$$

$$i = i_{0,V}\left(\frac{\theta}{\theta_0}\right)\frac{F}{RT}\eta \tag{15}$$

As the Tafel reaction is always in quasi-equilibrium we can also express Equation 7 in a more general form as

$$\theta = \frac{\left(\frac{k_{Td}}{k_{Tr}}\right)^{1/2}(c_{H_2})^{1/2}}{1+\left(\frac{k_{Td}}{k_{Tr}}\right)^{1/2}} \tag{16}$$

In the case of a very low fractional surface coverage, the denominator in Equation 16 is one. Subsequently, the fractional surface coverage will exhibit a square root dependency on the dissolved hydrogen concentration. The dissolved hydrogen concentration has no effect on the fractional surface coverage if it is already high.

Considering Equations 8, 15 and 16 it can be concluded that in the case of a very low fractional surface coverage the current density will be proportional to the square root of the dissolved hydrogen concentration. At a very high fractional surface coverage the current density becomes independent of the dissolved hydrogen concentration.

However, the Volmer exchange current density is dependent on the dissolved hydrogen concentration by shifts in the equilibrium potential (Equation 17, Nernst's law). Substituting Equation 17 into the anodic branch of Equation 8 shows this specific concentration dependency (Equation 18):

$$E_0 = E^{\blacklozenge} + \frac{RT}{2F}\ln\frac{[c_{H^+}]^2}{[c_{H_2}]} \quad (17)$$

$$i_{0,V} = Fk^{a}_{V,0}\exp\left[\alpha_V\frac{F}{RT}E^{\blacklozenge}\right](c_{H_2})^{-\alpha_V/2}(c_{H^+})^{\alpha_V}\theta_0 \quad (18)$$

Thus, taking this effect into account means that in the case of a very low fractional surface coverage the current density will show a concentration dependency equal to $(1-\alpha_V)/2$. At a very high fractional surface coverage the current density will show a concentration dependency equal to $-\alpha_V/2$.

2.2.3. *Approximate Volmer–Tafel mechanism*

Based on the foregoing analysis an approximate model to describe the current-potential behaviour is introduced. It follows from Equations 12 and 15 that for low overpotentials there exists a linear polarization relationship, regardless of the rate determining mechanism. Therefore, a general linear relationship between the current and the overpotential is proposed as given by Equation 19:

$$i = i^{ref}_{0,app}\left(\frac{c_{H_2}}{c^{ref}_{H_2}}\right)^{\gamma}\frac{F}{RT}\eta \quad (19)$$

The value of the apparent exchange current density will be determined by the relative influences of the Tafel and Volmer reactions (i.e., the reactivity of the electrode). The influence of the fractional surface coverage of adsorbed hydrogen atoms is described in terms of a dissolved hydrogen concentration dependency, as was analysed in the preceding Sections. This gives four possible limiting values of γ (Table 1).

As a reference equilibrium state in modelling the behaviour of the active layer of the gas diffusion electrode, the conditions at the gas–liquid interface are a logical choice. Because this reference equilibrium state is fixed, the concentration dependency of the Volmer exchange current density, due to shifts in the equilibrium potential, can be cancelled. This gives a different set of limiting values for γ, designated as γ^* (Table 2). Using the two extreme values of γ^*, one and zero, in further calculations, the whole domain of combinations between the rate determining step and the fractional surface coverage is accounted for.

Table 1. Limiting values of the concentration order γ for specific combinations of the rate determining step in the Tafel–Volmer hydrogen oxidation mechanism and extremes in the fractional surface coverage of adsorbed hydrogen atoms

Rate determining step	θ_{high}	θ_{low}
Tafel mechanism	0	1
Volmer mechanism	$-\alpha_V/2$	$(1-\alpha_V)/2$

Table 2. Limiting values of γ^*, the adjusted concentration order, for specific combinations of the rate determining step in the Tafel–Volmer hydrogen oxidation mechanism and extremes in the fractional surface coverage of adsorbed hydrogen atoms

Rate determining step	θ_{high}	θ_{low}
Tafel mechanism	0	1
Volmer mechanism	1	1/2

2.3. Mass and charge balances

To describe the mass and charge balances over the active layer, existing theory for the pseudohomogeneous description of porous electrodes is used [15, 16]. A general steady-state mass balance describes the changes in the dissolved hydrogen concentration, taking diffusion to be the only mass transfer mechanism:

$$D_{H_2,eff}\frac{d^2c_{H_2}}{dx^2} = \frac{a_e i}{2F} \quad (20)$$

Three additional current densities are introduced: a solution current density, j_s, a solid matrix current density, j_m, and a macroscopic current density, j_{macro}. These current densities are defined with respect to the geometric surface area of the gas diffusion electrode. The sum of the solution and solid matrix current densities is equal to the measurable macroscopic current density, j_{macro} (Equation 21). As the latter is always constant it follows that Equation 22 must hold, which is actually an expression of the electroneutrality condition:

$$j_{macro} = j_m + j_s \quad (21)$$

$$\frac{dj_m}{dx} = -\frac{dj_s}{dx} \quad (22)$$

A charge balance shows that charge leaving the solid phase must enter the solution phase (Equation 23). The electric potential in the solution phase will change due to the passage of current, as is described by Ohm's law (Equation 24). Combining Equations 23 and 24 gives a second order differential equation: a differential charge balance (Equation 25) [16]:

$$\frac{dj_s}{dx} = -\frac{dj_m}{dx} = a_e i \quad (23)$$

$$\frac{d\Phi_s}{dx} = -\frac{j_s}{\kappa_{eff}} \quad (24)$$

$$\frac{d^2\Phi_s}{dx^2} = -\frac{a_e i}{\kappa_{eff}} \quad (25)$$

2.4. Simulation of active layer behaviour

By substituting the kinetic equation (Equation 19) into the mass balance and the differential charge balance

(Equations 20 and 25), the behaviour of the active layer can be simulated. The overpotential in the kinetic equation is substituted by Equation 26. Because the hydrogen oxidation takes place at standard conditions the equilibrium potential will be equal to zero, Φ_m is arbitrarily set to zero:

$$\eta = E - E_0 = (\Phi_m - \Phi_s) - E_0 = -\Phi_s \tag{26}$$

Both the mass balance and the differential charge balance can be written in dimensionless form (Equations 27–30). Two solutions exist for this system of second order differential equations depending on the value used for the concentration order, γ^*.

$$\xi = \frac{x}{L}, \quad c^*_{H_2} = \frac{c_{H_2}}{c^{ref}_{H_2}}, \quad \Phi^*_s = \frac{F}{RT}\Phi_s \tag{27}$$

$$K1 = \frac{a_e i^{ref}_{0,app}(L)^2}{2FD_{H_2,eff}c^{ref}_{H_2}}, \quad K2 = \frac{a_e i^{ref}_{0,app}(L)^2 F}{RT\kappa_{eff}} \tag{28}$$

$$\frac{d^2 c^*_{H_2}}{d\xi^2} = -K1\left(c^*_{H_2}\right)^{\gamma^*}\Phi^*_s \tag{29}$$

$$\frac{d^2 \Phi^*_s}{d\xi^2} = K2\left(c^*_{H_2}\right)^{\gamma^*}\Phi^*_s \tag{30}$$

For the solution with γ^* equal to one, the boundary conditions are postulated in Equations 31 and 32. The solution phase potential at $\xi = 1$ represents the (externally) applied overpotential which is measured against a suitable reference electrode placed in the bulk of the electrolyte solution. This potential is corrected for the ohmic potential drop between the reference electrode and the outside surface of the active layer [17]. The boundary condition for the slope of the concentration profile at $\xi = 1$, which introduces the mass transfer Biot number, follows from consideration of the external mass transfer resistance [18]:

$$\xi = 0 \Rightarrow \frac{d\Phi^*_s}{d\xi} = 0, \quad c^*_{H_2} = 1 \tag{31}$$

$$\xi = 1 \Rightarrow \Phi^*_s = \Phi^*_s(1), \quad \frac{dc^*_{H_2}}{d\xi} = -Bi_m c^*_{H_2}(1) \tag{32}$$

The set of equations for $\gamma^* = 1$ cannot be solved analytically. A numerical finite difference method (DO2RAF) [19] was used to approximate the solution. For the solution with γ^* equal to zero, two solutions are possible depending on the penetration depth of dissolved hydrogen into the active layer of the electrode. This distinction is analogous to the treatment of ordinary zero-order chemical reactions in a porous catalyst [20]. In the case of full penetration, the boundary conditions are exactly the same as formulated in Equations 31 and 32. The second solution considers partial penetration of the active layer, up to a certain penetration depth λ. The boundary conditions at $\xi = 1$ do not longer apply and a new set of boundary conditions are formulated as given by Equation 33. The condition for the gradient in the solution phase potential at $\xi = \lambda$ follows from consideration of Ohm's law for $\xi > \lambda$. For $\xi > \lambda$ the reaction current density will be equal to zero, which means that the solution current density becomes constant (Equation 23) and the potential gradient for $\lambda \leqslant \xi \leqslant 1$ is linear (Equation 24) with a slope as given by Equation 33:

$$\xi = \lambda \Rightarrow \frac{d\Phi^*_s}{d\xi} = \frac{\Phi^*_s(1) - \Phi^*_s(\lambda)}{1-\lambda}, \quad \frac{dc^*_{H_2}}{d\xi} = 0, \quad c^*_{H_2} = 0 \tag{33}$$

In both cases of γ^* equal to zero an analytical solution for the system of second order differential equations has been derived (Appendix). The solution phase potential and the dissolved hydrogen concentration profiles in the case of a fully penetrated active layer can be described using Equations 34 and 35.

$$\Phi^*_s(\xi) = \frac{\Phi^*_s(1)\cosh\left(\sqrt{K2}\xi\right)}{\cosh\left(\sqrt{K2}\right)} \tag{34}$$

$$c^*_{H_2}(\xi) = 1 + \frac{K1\Phi^*_s(1)\left(1-\cosh\left(\sqrt{K2}\xi\right)\right)}{K2\cosh\left(\sqrt{K2}\right)} + \left(\frac{\xi Bi_m}{1+Bi_m}\right) \times \left(\frac{K1\Phi^*_s(1)}{K2}\left(1 - \frac{1}{\cosh\left(\sqrt{K2}\right)} + \frac{K2\tanh\left(\sqrt{K2}\right)}{Bi_m}\right) - 1\right) \tag{35}$$

In the case of partial penetration of the active layer Equations 36 and 37 should be used for $0 \leq \xi \leq \lambda$. The penetration depth at the prevailing process conditions (i.e., values of $K1$, $K2$ and η) can be determined numerically by solving Equation 38. Thus,

$$\Phi^*_s(\xi) = \frac{\Phi^*_s(1)\cosh\left(\sqrt{K2}\xi\right)}{\cosh\left(\sqrt{K2}\lambda\right) + (1-\lambda)\sqrt{K2}\sinh\left(\sqrt{K2}\lambda\right)} \tag{36}$$

$$c^*_{H_2}(\xi) = \frac{K1\Phi^*_s(1)\left(-\cosh\left(\sqrt{K2}\xi\right) + (\xi-\lambda)\sqrt{K2}\sinh\left(\sqrt{K2}\lambda\right) + \cosh\left(\sqrt{K2}\lambda\right)\right)}{K2\cosh\left(\sqrt{K2}\lambda\right) + (1-\lambda)(K2)^{3/2}\sinh\left(\sqrt{K2}\lambda\right)} \quad (37)$$

$$1 - \left(\frac{K1i\Phi^*_s(1)\left(-1-\lambda\sqrt{K2}\sinh\left(\sqrt{K2}\lambda\right) + \cosh\left(\sqrt{K2}\lambda\right)\right)}{K2\cosh\left(\sqrt{K2}\lambda\right) + (1-\lambda)(K2)^{3/2}\sinh\left(\sqrt{K2}\lambda\right)}\right) = 0 \quad (38)$$

For both values of γ^*, the macroscopic current density can be calculated indirectly from the slope of the solution phase potential at $\xi = 1$ using Equation 24 and the fact that $j_{macro} = j_s$ at that point. It is also possible to determine the macroscopic current density by numerical integration of the local reaction current densities over the active layer thickness.

3. Results

3.1. Comparison with experimental data

Simulation results are compared with experimental polarization curves of electrodes with different reactivities obtained by Vermeijlen et al. [12, 13]. They concluded that it was possible to fit these data for an overpotential range of 15 mV to a linear macroscopic equation (Equation 39). Examples of these polarization curves, using experimental values of the apparent exchange current density taken from Vermeijlen et al. [13], are shown in Figure 2.

$$j_{macro} = j^{exp}_{0,app}\frac{F}{RT}\eta \quad (39)$$

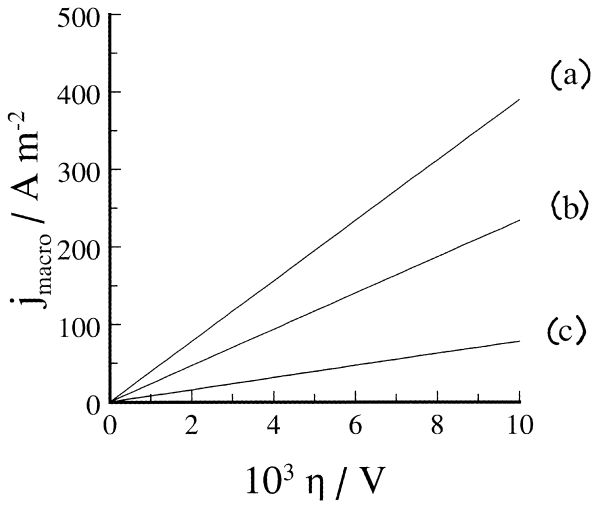

Fig. 2. Polarization curves based on Equation 39 and experimental apparent exchange current densities determined by Vermeijlen et al. (Figure 9 [13]), corresponding with different electrode reactivities. $j^{exp}_{0,app}$: (a) 1000, (b) 600 and (c) 200 A m^{-2}.

3.2. Simulation results

The behaviour of the active layer was simulated using both values of γ^* and a characteristic set of data for the process conditions (Table 3). The simulations were initially performed with a very high Biot mass number, so the influence of the external mass transfer resistance was neglected. Both the effective solution conductivity and the effective dissolved hydrogen diffusion coefficient were calculated using the Bruggeman equation:

$$\kappa_{eff} = \kappa\varepsilon^{3/2}, \quad D_{eff} = D\varepsilon^{3/2} \quad (40)$$

Experimental results obtained by Vermeijlen [12, 13] show a strong linear behaviour of the macroscopic current density as a function of applied overpotential in the region between 0–100 mV. However, our initial simulations showed a moderate curvature of the macroscopic current density as a function of applied overpotential. This effect contributes to underestimation of the ohmic resistance in the solution phase [23], due to overestimation of the porosity of the active layer or the correction of the solution conductivity by the Bruggeman equation which is not appropriate in this case. Nevertheless, acceptable linearity was obtained by using an estimated porosity of 0.25 combined with the Bruggeman equation. This value and correction method were used in further calculations.

In Figure 3 calculated profiles of the macroscopic current density as a function of the applied overpotential are shown for different values of electrode reactivity. The calculated profiles cover the current density range corresponding with the experimental polarization curves shown in Figure 2. The profiles of the dissolved hydrogen concentration and the solution phase potential at a very low macroscopic current density and electrode reactivity are shown in Figure 4. These profiles show that the activity is mostly located at the gas–liquid interface.

As the active layer of the gas diffusion electrode will, usually, be only partly penetrated with dissolved hydrogen at realistic operating conditions, external mass transfer into the bulk of the electrolyte does not need to be considered.

A critical operating condition is reached when the active layer becomes just fully penetrated with dissolved hydrogen. Subsequently, leakage of dissolved hydrogen gas into the main stream of liquid electrolyte can occur due to small shifts in the operating regime. Obviously, the conversion of dissolved hydrogen gas into protons will then no longer be complete.

The critical operating conditions for both values of γ^* have been determined. A critical condition is defined as

Table 3. Characteristic process conditions used in simulating the behaviour of the gas diffusion electrode

Parameter	Value	Unit
Active layer thickness	1×10^{-4}	m
Porosity of active layer	0.25	–
Electrolyte concentration (H_2SO_4)	1000	mol m^{-3}
Solution conductivity*	40	Ω^{-1} m^{-1}
Dissolved H_2 diffusion coefficient	3×10^{-9}	m^2 s^{-1}
Hydrogen gas pressure	1	atm
Dissolved H_2 reference concentration†	0.67	mol m^{-3}
Biot number	1000	–
Temperature	298	K

* Data from Lobo [21].
† Data from Battino et al. [22].

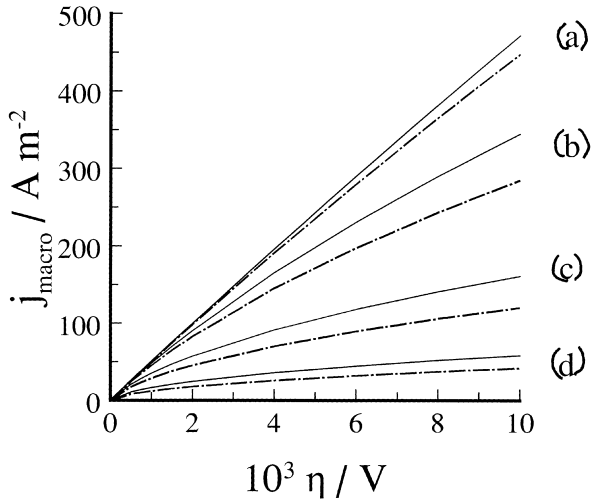

Fig. 3. Simulated macroscopic current densities as a function of externally applied overpotential for $\gamma^* = 1$ (broken lines) and $\gamma^* = 0$ (full lines) and various electrode reactivities. $a_e i^{ref}_{0,app}$: (a) 10^{11}, (b) 10^{10}, (c) 10^9 and (d) 10^8 A m^{-3}.

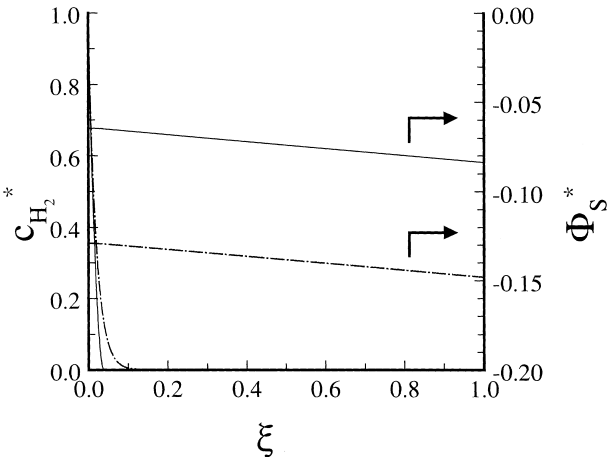

Fig. 4. Dissolved hydrogen concentration and solution phase potential profiles for $\gamma^* = 1$ (broken lines) and $\gamma^* = 0$ (full lines). With $j_{macro} = 25$ A m^{-2} and $a_e i^{ref}_{0,app} = 10^8$ A m^{-3}.

the combination of values for *K1*, *K2* and the applied overpotential for which the flux of dissolved hydrogen from the active layer into the main stream of liquid electrolyte is just equal to zero. This corresponds to a 100% fractional conversion of hydrogen gas fed to the reactor. For $\gamma^* = 0$ the critical values of the three parameters can be determined using Equation 38. The critical operating condition arises when λ becomes equal to one. By specifying two process parameters it is then possible to calculate the value of the third parameter. In Figure 5 the results are reported of varying the process parameters over a considerable range of values. Based on these data an empirical formula was fitted by which the critical operating conditions can be determined:

$$K1 = \frac{1}{\eta}\left(\frac{4}{1 + \left(\frac{10^4}{K2}\right)^{0.6}} + 0.048\right) \tag{41}$$

With $\gamma^* = 1$ a critical operating condition arises when the flux of hydrogen from the active layer is just equal to zero. However, in the case of a first order concentration dependency of the reaction rate, the concentration

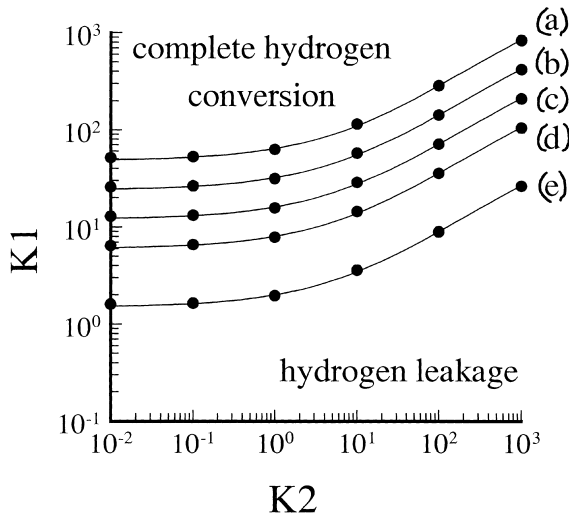

Fig. 5. Combinations of *K1*, *K2* and η for which critical process conditions arise in the case of $\gamma^* = 0$. Calculated values are given by dots, drawn lines correspond with Equation 41. η: (a) 0.001, (b) 0.002, (c) 0.004, (d) 0.008 and (e) 0.032 V.

can never reach zero. Thus, there is always a flux of dissolved hydrogen from the active layer. In case of $\gamma^* = 1$ the definition of the critical operating condition was therefore modified by stating that it corresponds to a fractional conversion of dissolved hydrogen just higher then 99.9%. The fractional conversion of dissolved hydrogen gas can be calculated from the fluxes at $\xi = 0$ and $\xi = 1$:

$$\Gamma_{H_2} = \frac{\left.\frac{dc^*_{H_2}}{d\xi}\right|_{\xi=0} - \left.\frac{dc^*_{H_2}}{d\xi}\right|_{\xi=1}}{\left.\frac{dc^*_{H_2}}{d\xi}\right|_{\xi=0}} \tag{42}$$

In Figure 6 the critical combinations of parameters are shown. Also in this case an empirical formula (Equation 43) has been fitted by which the critical operating conditions can be estimated. In the calculations a high Biot number (i.e., 1000) was used. This corresponds to an extremely high mass transfer rate from the active layer. For lower Biot numbers, the critical operating conditions predicted by Equation 43 lead to situations with a fractional conversion well over 99.9%.

$$K1 = \frac{1}{\eta}\left(\frac{33.6}{1 + \left(\frac{3442}{K2}\right)^{0.58}} + 1.51\right) \tag{43}$$

4. Discussion

The derived concentration dependencies of the extreme situations arising in the Volmer–Tafel mechanism, by means of γ, agree perfectly with the results of theoretical calculations reported by Vermeijlen et al. (Figure 5 in [13]). These authors presented calculations for the concentration dependency of the complete Volmer–Tafel mechanism, for various combinations of the reaction rates of both the Tafel and Volmer reaction. From their graphs, the concentration dependency of the Volmer–Tafel mechanism in the extreme situations can be deduced. Our treatment shows that these findings can be derived from the basic equations.

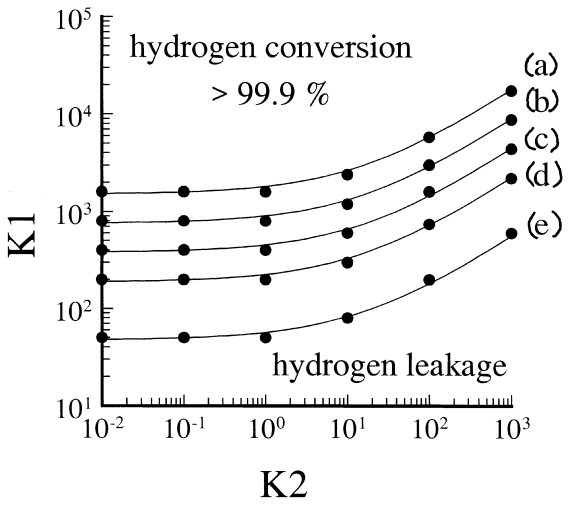

Fig. 6. Combinations of $K1$, $K2$ and η for which critical process conditions arise in the case of $\gamma^* = 1$. Calculated values are given by dots, drawn lines correspond with Equation 43. η: (a) 0.001, (b) 0.002, (c) 0.004, (d) 0.008 and (e) 0.032 V.

The error introduced by the linearization procedure applied in this paper depends on the overpotential range studied in combination with the reactivity of the gas diffusion electrode. If the reactivity of the electrode is low then the Tafel reaction will have a considerable influence on the oxidation rate. In that case the error is mostly determined by the linearization of Equation 12, which grows rapidly with increasing overpotential values. To keep the error within reasonable margins (i.e., less than 30%) the model should in those circumstances not be used for overpotentials over 10 mV. In case of an electrode with a high reactivity the Volmer reaction will be rate determining, so the error will be due to linearization of Equation 14. The range of application of the model can then be extended to values of the overpotential of approximately 40 mV, while maintaining reasonable error margins (i.e., less than 10%).

The estimate of the value of the effective solution phase conductivity in the active layer of the gas diffusion electrode by means of the Bruggeman equation can be considered doubtful. The reason for this is that the geometry of the active layer can be considered as very complex in comparison with the dispersions for which the Bruggeman equation was originally derived [24]. A more suitable correlation for the effective solution conductivity, even as an accurate value for the porosity of the active layer of the gas diffusion electrode, were not obtained. Determination of these parameters lies beyond the scope of the present research. Therefore, the procedure to estimate the effective conductivity in the active layer on the basis of the shape of the experimental polarization curves seems justified.

The order of magnitude of the values of the reactivity parameter, $a_e i^{ref}_{0,app}$, necessary to match the simulated and the experimental polarization curves seems to comply with other reported values. The value used for the most reactive electrode, 10^{11} A m^{-3}, agrees perfectly with the value reported by Bernardi and Verbrugge for a solid polymer electrolyte fuel cell (SPEFC) anode, for which they assumed the Volmer reaction step to be rate determining [11].

Severe mass transfer limitations inside the active layer have also been reported for other types of gas diffusion electrodes, concerning the hydrogen oxidation as well as oxygen reduction [10, 11, 25]. However, in the cases concerning the hydrogen oxidation, only the Volmer reaction was taken into account. It has now been shown that even with a lower reactivity this limitation still holds, although it must be emphasized that the thickness of the active layer is of course an important parameter in that respect. In this work a PAFC type of gas diffusion electrode was studied with an active layer thickness of approximately 10^{-4} m. In the case of SPEFC electrodes this value may be ten times smaller [11], so the relative

penetration depth of dissolved hydrogen at a certain electrode reactivity, will be much greater.

A decrease in the active layer thickness means a decrease in the ohmic potential drop in the solution phase, making the process more energy efficient. However, in low current density applications of a gas diffusion anode hydrogen leakage is possible. The analysis of the critical operating conditions at which dissolved hydrogen leakage occurs, has resulted in empirical formulae by which the risk of leakage can be easily assessed.

The observation that current is mainly produced at the gas–liquid interface justifies further simplification of the model: the reactive plane approximation. In this approach mass transfer of dissolved hydrogen into the active layer is considered to be insignificant and the entire reaction current is produced at the reactive plane. There, the dissolved hydrogen concentration will be equal to the maximum solubility concentration of hydrogen gas in the electrolyte solution. It should be noted that similar descriptions have been presented for gas-liquid absorption systems with fast chemical reaction in the liquid phase [26].

Using the reactive plane approximation it follows from Equation 19 that the two different values of γ^* will give identical results. Thus, the reactivity of the electrode is expressed solely by the value of the apparent exchange current density, $i_{0,\mathrm{app}}^{\mathrm{ref}}$. The apparent exchange current density, which is based on the true electroactive surface area, can be substituted by a more accessible parameter, $j_{0,\mathrm{app}}^{\mathrm{ref}}$, which is based on the geometric surface area. The value of this parameter is equal to $j_{0,\mathrm{app}}^{\mathrm{ref}}$, and it can be directly obtained from measuring the macroscopic current density as a function of applied overpotential (see Equation 39). The gradient of the solution potential over the active layer will be constant and is obtained by simple integration of Equation 24 over the active layer thickness and taking $j_{\mathrm{s}} = j_{\mathrm{macro}}$:

$$\Delta\Phi_{\mathrm{s}} = \int_0^L \mathrm{d}\Phi_{\mathrm{s}} = \int_0^L -\frac{j_{\mathrm{s}}}{\kappa_{\mathrm{eff}}} = -\frac{j_{\mathrm{macro}}L}{\kappa_{\mathrm{eff}}} \qquad (44)$$

Acknowledgement

Prof. dr ir A.A.H. Drinkenburg is acknowledged for his comments and reading of this manuscript. The authors gratefully acknowledge the support of this research by the Technology Foundation (Technologiestichting S.T.W.), The Netherlands.

References

1. L.J.J. Janssen, *Dutch Patent 9 101 022* (1991).
2. E.C.W. Wijnbelt and L.J.J. Janssen, *J. Appl. Electrochem.* **24** (1994) 1028–34.
3. I. Portegies Zwart and L.J.J. Janssen, *J. Appl. Electrochem.* **28** (1998) 1–9
4. I. Portegies Zwart, E.C.W. Wijnbelt and L.J.J. Janssen, *in* Y.S. Fung, T.T. Kam and K.A. Klun (Eds), Proceedings of the Symposium on 'Electrochemical Science and Technology', Hong Kong (1995) L-75.
5. K.N. Njau, W.-J. van der Knaap and L.J.J. Janssen, *J. Appl. Electrochem.* **28** (1998) 343–49.
6. I. Portegies Zwart, J.K.M. Jansen and L.J.J. Janssen, *J. Appl. Electrochem.* (2000) was submitted.
7. J. Giner and C. Hunter, *J. Electrochem. Soc.* **116** (1969) 1124–30.
8. M.B. Cutlip, S.C. Yang and P. Stonehart, *Electrochim. Acta* **36** (1991) 547–53.
9. P. Stonehart and P.N. Ross, *Electrochim. Acta* **21** (1976) 441–45.
10. T.E. Springer, M.S. Wilson and S. Gottesfeld, *J. Electrochem. Soc.* **140** (1993) 3513–26
11. D.M. Bernardi and M.W. Verbrugge, *J. Electrochem. Soc.* **139** (1992) 2477–91.
12. J.J.T.T. Vermeijlen, PhD thesis, Eindhoven University of Technology, Eindhoven (1994).
13. J.J.T.T. Vermeijlen, L.J.J. Janssen and G.J. Visser, *J. Appl. Electrochem.* **27** (1997) 497–506.
14. K.J. Vetter, 'Elektrochemische Kinetik' (Springer-Verlag, Berlin, 1961), pp. 410–21.
15. J. Newman and W. Tiedemann, *A.I.Ch.E.* **21** (1975) 25–41
16. F. Coeuret and A. Storck, 'Elements de Genie Electrochimique' (Technique et Documentation (Lavoisier), Paris, 1984), pp. 279–321
17. C. Lagergren, G. Lindbergh and D. Simonsson, *J. Electrochem. Soc.* **142** (1995) 787–97
18. J.J. Carberry, *in* J.R. Anderson and M. Boudart (Eds), 'Catalysis, Science and Technology', Volume 8 (Springer-Verlag, Berlin, 1987), pp. 131–71
19. Numerical Algorithms Group Ltd, 'NAG Fortran Library Manual', Mark 16, Volume 2: 'Ordinary Differential Equations' (NAG, Oxford, 1993).
20. A.E. Rodrigues, J.M. Órfao and A. Zoulalian, *Chem. Eng. Commun.* **27** (1984) 327–37.
21. V.M.M. Lobo, 'Handbook of Electrolyte Solutions' (Elsevier, Amsterdam, 1989), p. 668.
22. R. Battino, H.L. Clever and C.L. Young, *in* C.L. Young, (Ed.), 'Solubility Data Series', Volume 5/6 (Pergamon Press, Oxford, 1981), p. 37.
23. L.J. Ryan and J.R. Selman, *in* H.C. Maru, T. Katan and M.G. Klein, (Eds), Proceedings of the symposium on 'Porous electrodes: theory and practice', Volume 84 - 8, The Electrochemical Society, Pennington, NJ (1984), pp. 377–95.
24. R.E. Meredith and C. Tobias, *in* P. Delahay and C.W. Tobias, (Eds), 'Advances in Electrochemistry and Electrochemical Engineering', Volume 2 (Interscience, New York, 1962), pp. 15–47.
25. K. Broka and P. Ekdunge, *J. Appl. Electrochem.* **27** (1997) 281–89.
26. K.R. Westerterp, W.P.M. van Swaaij and A.A.C.M. Beenackers, 'Chemical Reactor Design and Operation' (Wiley & Sons, New York, 1995).

Appendix: Analytical solutions for the concentration and solution phase potential profiles in the active layer for $\gamma^* = 0$

Full penetration of active layer

The trial solution for Equation 30 is chosen as

$$\Phi_{\mathrm{s}}^* = A\cosh(\sqrt{K2}\xi) + B\sinh(\sqrt{K2}\xi) \qquad (A1)$$

Differentiating Equation A1 and using boundary Equation 31 gives the value of constant B, which is equal to zero. Using this value in Equation A1 together with the second boundary condition (Equation 32) gives the value of A. The final solution for Equation 30 can then be written as Equation A3.

$$A = \frac{\Phi_s^*(1)}{\cosh(\sqrt{K2})} \tag{A2}$$

$$\Phi_s^*(\xi) = \frac{\Phi_s^*(1)\cosh(\sqrt{K2}\xi)}{\cosh(\sqrt{K2})} \tag{A3}$$

Equation A3 can be substituted in Equation 29 to give Equation A4, which by double integration transforms to Equation A5.

$$\frac{d^2 c_{H_2}^*}{d\xi^2} = -\frac{K1\Phi_s^*(1)\cosh(\sqrt{K2}\xi)}{\cosh(\sqrt{K2})} \tag{A4}$$

$$c_{H_2}^*(\xi) = -\frac{K1\Phi_s^*(1)\cosh(\sqrt{K2}\xi)}{K2\cosh(\sqrt{K2})} + C1\xi + C2 \tag{A5}$$

The second integration constant, $C2$, follows from considering boundary Equation 31 and Equation A5. The first integration constant, $C1$, follows from Equation 32 combined with Equations A5, A6 and the differentiated version of Equation A5.

$$C2 = 1 + \frac{K1\Phi_s^*(1)}{K2\cosh(\sqrt{K2})} \tag{A6}$$

$$C1 = \left(\frac{Bi_m}{1+Bi_m}\right)\left(\frac{K1\Phi_s^*(1)}{K2}\left(1 - \frac{1}{\cosh(\sqrt{K2})} + \frac{K2\tanh(\sqrt{K2})}{Bi_m}\right) - 1\right) \tag{A7}$$

The final solution can subsequently be expressed by Equation A8.

$$c_{H_2}^*(\xi) = 1 + \frac{K1\Phi_s^*(1)(1-\cosh(\sqrt{K2}\xi))}{K2\ \cosh(\sqrt{K2})} + \left(\frac{\xi Bi_m}{1+Bi_m}\right)\left(\frac{K1\Phi_s^*(1)}{K2}\left(1 - \frac{1}{\cosh(\sqrt{K2})} + \frac{K2\tanh(\sqrt{K2})}{Bi_m}\right) - 1\right) \tag{A8}$$

Partial penetration of active layer

Again a trail solution for Equation 30 is used as given by Equation A1. The boundary condition given by Equation 31 also applies in this case, thus constant B is equal to zero. Using this value in the differentiated version of Equation A1 together with the second boundary condition, Equation 33, the value of A can be determined (Equation A9). The dimensionless solution potential at λ can be eliminated by substituting Equation A9 into Equation A1 (including $B = 0$) and solving for $\xi = \lambda$. After some rearrangement the final solution is given by Equation A10. This solution reduces nicely to Equation A3 for $\lambda = 1$.

$$A = \frac{\Phi_s^*(1) - \Phi_s^*(\lambda)}{(1-\lambda)\sqrt{K2}\ \sinh(\sqrt{K2}\lambda)} \tag{A9}$$

$$\Phi_s^*(\xi) = \frac{\Phi_s^*(1)\ \cosh(\sqrt{K2}\xi)}{\cosh(\sqrt{K2}\lambda) + (1-\lambda)\sqrt{K2}\ \sinh(\sqrt{K2}\lambda)} \quad \text{for } 0 \leqslant \xi \leqslant \lambda \tag{A10}$$

Equation A10 can be substituted in Equation 29 to give Equation A11, which after double integration transforms to Equation A12.

$$\frac{d^2 c_{H_2}^*}{d\xi^2} = -\frac{K1\Phi_m^*(1)\ \cosh(\sqrt{K2}\xi)}{\cosh(\sqrt{K2}\lambda) + (1-\lambda)\sqrt{K2}\ \sinh(\sqrt{K2}\lambda)} \tag{A11}$$

$$c_{H_2}^*(\xi) = -\frac{K1\Phi_s^*(1)\ \cosh(\sqrt{K2}\xi)}{K2\ \cosh(\sqrt{K2}) + (1-\lambda)(K2)^{3/2}\ \sinh(\sqrt{K2}\lambda)} + C1\xi + C2 \tag{A12}$$

The first integration constant, $C1$, follows from considering the condition for the gradient of the concentration at λ (boundary Equation 33), together with the differentiated version of Equation A12:

$$C1 = \frac{K1\Phi_s^*(1)\ \sinh(\sqrt{K2}\lambda)}{\sqrt{K2}\ \cosh(\sqrt{K2}\lambda) + (1-\lambda)K2\ \sinh(\sqrt{K2}\lambda)} \tag{A13}$$

The second integration constant can be determined by inserting Equation A13 into Equation A12 and subsequently using the condition for the concentration at λ (boundary Equation 33):

$$C2 = \frac{K1\Phi_s^*(1)\ \cosh(\sqrt{K2}\lambda) - \lambda\sqrt{K2}K1\Phi_s^*(1)\ \sinh(\sqrt{K2}\lambda)}{\sqrt{K2}\ \cosh(\sqrt{K2}\lambda) + (1-\lambda)(K2)^{3/2}\ \sinh(\sqrt{K2}\lambda)} \tag{A14}$$

The final solution for $0 \leqslant \xi \leqslant \lambda$ can then be expressed as

$$c_{H_2}^*(\xi) = \frac{K1\Phi_s^*(1)\left(-\cosh(\sqrt{K2}\xi) + (\xi-\lambda)\sqrt{K2}\ \sinh(\sqrt{K2}\lambda) + \cosh(\sqrt{K2}\lambda)\right)}{K2\ \cosh(\sqrt{K2}\lambda) + (1-\lambda)(K2)^{3/2}\sinh(\sqrt{K2}\lambda)} \tag{A15}$$

The penetration depth, λ, is the only unknown left in Equations A10 and A15. By using boundary Equation 33 together with Equation A15 an algebraic equation is constructed with only one unknown, the penetration depth (Equation A16). It can be solved numerically to give a value for λ.

$$1 - \left(\frac{K1\Phi_s^*(1)(-1 - \lambda\sqrt{K2}\ \sinh(\sqrt{K2}\lambda) + \cosh(\sqrt{K2}\lambda))}{K2\ \cosh(\sqrt{K2}\lambda) + (1-\lambda)(K2)^{3/2} \sinh(\sqrt{K2}\lambda)} \right) = 0 \quad \text{(A16)}$$